Journal of Power Sources 267 (2014) 203–211

Contents lists available at ScienceDirect

Journal of Power Sources

journal homepage: www.elsevier.com/locate/jpowsour

LiF/Fe/V_2O_5 nanocomposite as high capacity cathode for lithium ion batteries

B. Das [a, b, *], A. Pohl [b], V.S.K. Chakravadhanula [a, c], C. Kübel [a, b, c], M. Fichtner [a, b, *]

[a] Helmholtz Institute Ulm (HIU), Albert-Einstein Allee 11, D-89081 Ulm, Germany
[b] Karlsruhe Institute of Technology, Institute of Nanotechnology, D-76021 Karlsruhe, Germany
[c] Karlsruhe Nano Micro Facility (KNMF), Karlsruhe Institute of Technology, D-76021 Karlsruhe, Germany

HIGHLIGHTS

- We prepared LiF/Fe/V_2O_5 nanocomposite in discharge state for practical application as cathode by simple ball milling method.
- The composite showed high reversible capacity.
- Heat-treated nanocomposite showed high and stable capacity.
- We performed ex-situ TEM and -XRD to support reaction mechanism.
- Electrochemical impedance spectroscopy (EIS) was carried out to understand the electrode kinetics.

ARTICLE INFO

Article history:
Received 6 November 2013
Received in revised form
7 April 2014
Accepted 7 May 2014
Available online 21 May 2014

Keywords:
Iron fluoride
Conversion materials
Nanocomposite
Electrochemical impedance spectroscopy
Lithium ion batteries

ABSTRACT

Iron fluoride based conversion cathode materials, LiF/Fe/V_2O_5 nanocomposites with high activity and good cyclic stability have been prepared in the discharged state by employing high energy ball milling and characterized by using XRD, SEM and TEM techniques. Li cycling behavior have been investigated by using galvanostatic cycling and cyclic voltammetry. It has been inferred that addition of V_2O_5 significantly enhanced the performance of the LiF/Fe nanocomposites by improving its electronic as well as its ionic conductivity. LiF/Fe/V_2O_5 (15 wt.%, 30 h ball milled) shows the best cycling performance. A high first cycle discharge capacity of ~510 (±5) mA h g^{-1} is observed. At the end of 50th cycle, the capacity observed is ~270 (±5) mA h g^{-1}. The heat treated LiF/Fe/V_2O_5 (15 wt.%, 20 h ball milled) nanocomposite shows a notable improvement in cycling stability than the as prepared nanocomposite and a reversible capacity of ~310 (±5) mA h g^{-1} is observed at the end of 50 cycles. The average charge–discharge potentials observed in CV are ~2.9 and ~1.7 V, respectively. Ex-situ XRD, TEM and EIS measurements are performed on cycled electrodes of LiF/Fe/V_2O_5 (15 wt.%; 30 h ball milled) at selected voltages to understand the reaction mechanism.

1. Introduction

Lithium ion batteries (LIBs) are used as secondary energy/power sources for portable electronic devices and they are expected to play an important role for automobile industries [1,2]. However, their low energy density is a major issue for their extensive practical applications. The current state-of-art LIBs use layered Li transition metal oxides (sp. capacity ~150 mA h g^{-1} for $LiCoO_2$) [3,4] and olivine type $LiFePO_4$ (sp. capacity ~170 mA h g^{-1}) [5,6] as cathode materials. These materials show excellent electrochemical cycling performance and undergo Li ion intercalation process where a maximum up to 1Li^+ can be reversibly stored during charge/discharge process, yielding in limited specific capacity and limited energy density. In order to achieve higher energy density, utilization of higher oxidation states of transition metals is required. Cathodes based on conversion reaction appear to be potential candidates which involve multi-electron redox reaction and theoretically deliver a high specific capacity. Metal fluorides, MF_3 (M = Fe, Co, Ni, V, Mn, Ti etc.) are interesting options as cathodes due to their high voltage and high theoretical specific capacity, which is at least 4 times higher than the capacity of $LiCoO_2$ and $LiFePO_4$ [7–9].

* Corresponding authors. Helmholtz Institute Ulm (HIU), Albert-Einstein Allee 11, D-89081 Ulm, Germany. Tel.: +49 721 608 28924, +49 721 608 25340.
E-mail addresses: bijoy.das@kit.edu (B. Das), maximilian.fichtner@kit.edu (M. Fichtner).

http://dx.doi.org/10.1016/j.jpowsour.2014.05.063
0378-7753/

Iron fluoride appears to be an attractive cathode material due to its low cost, high reversible capacity (theoretical capacity: 712, 571 mA h g^{-1} for FeF_3 and FeF_2 respectively) and eco-friendliness. Additionally, the thermal stability when mixed with an electrolyte would be another advantage of FeF_3 for its large-scale application [10]. FeF_3 has a ReO_3-type crystal structure [8], and hence, electrochemical Li ion intercalation (1 e^- transfer) (Eq. (1)) is facilitated due to its open structure followed by its conversion to form LiF and Fe metal ($2e^-$ transfer) (Eq. (2)) [11].

$$FeF_3 + Li^+ + e^- \rightarrow LiFeF_3 \quad (1)$$

$$LiFeF_3 + 2Li^+ + 2e^- \rightarrow Fe^0 + 3LiF \quad (2)$$

$$FeF_3 + 3Li^+ + 3e^- \leftrightarrow Fe^0 + 3LiF \quad (3)$$

Hence, the reversible capacity of FeF_3 (Eq. (3)) exceeds that of layered Li metal oxides and phosphates.

The electrochemical performance of FeF_3 was first reported by Arai et al. [12] and a reversible capacity of ~80 mA h g^{-1} was shown for the Fe^{3+}/Fe^{2+} reversible reaction in the voltage window of 2.0–4.5 V. The low intrinsic conductivity was found to be a major problem leading to poor electrochemical performance which would have to be improved before using it as a cathode material for LIBs. Addition of conducting reagents to FeF_3 is an effective approach to enhance the conductivity of FeF_3 and to improve the electrochemical performance. In 2003, Badway et al. [13] reported an improved electrochemical performance of ball milled FeF_3/C composite and they showed a high reversible capacity of ~600 mA h g^{-1} for Fe^{3+}/Fe^0 redox couple in the voltage range of ~1.5–4.5 V at 7.58 mA g^{-1} current density. Li et al. [11] prepared FeF_3/C nanocrystals by different chemical routes and showed a high reversible capacity even at high current rate (2000 mA g^{-1}). Kung et al. [14] synthesized FeF_3/rGO (reduced graphene oxide) composite using a facile self-assembly approach combined with photo thermal reduction and reported a high initial capacity of ~580 mA h g^{-1} after 10 cycles for FeF_3/rGO in the voltage window of 1.0–4.5 V at 100 mA g^{-1} for Fe^{3+}/Fe^0 redox couple. Recently, Liu et al. [15] synthesized FeF_3 on reduced graphene sheet through a low temperature solution phase route and showed a stable capacity of ~210 mA h g^{-1} at 0.2 C rate in the voltage window of 2.0–4.5 V for Fe^{3+}/Fe^{2+} redox couple. When cycled at 0.1 C in the voltage window 1.5–4.5 V, FeF_3/graphene reported to exhibit a stable capacity of ~490 mA h g^{-1} up to 20 cycles. Recently, Reddy et al. [16] reported CFx derived C–FeF_2 nanocomposite, prepared from thermal decomposition of $Fe(CO)_5$ in the presence of CFx, where FeF_2 nanoparticles were encapsulated by graphitic carbon.

Badway et al. suggested that mixed conducting matrices (MCM) can be prepared by adding electrochemically active materials, such as $MoO_{3-\delta}$, V_2O_5 or MoS_2 to transition metal fluorides, to enhance the transport of both lithium ions as well as electrons to attain improved electrochemical performance [17]. They prepared CuF_2/MCM (MCM = MoO_3, VO_2, V_2O_5, MoO_2, CuO and NiO) composites and reported improved electrochemical performance compared to pure CuF_2. CuF_2/V_2O_5 composite showed ~300 mA h g^{-1} when cycled at 7.58 mA g^{-1}, which is higher than that of pure CuF_2 (100 mA h g^{-1}) [17]. Wu et al. reported the preparation of FeF_3/V_2O_5 [18] and FeF_3/MoS_2 [19] composites by ball milling and showed that these composites exhibiting improved Li cycling performance compared to pure FeF_3. Although nanostructured FeF_3 and its nanocomposites with conducting reagents showed improved electrochemical performance, they cannot be directly used as cathode with non-lithium anode materials for rechargeable LIBs due to absence of Li in the material. Hence, it is essential to prepare the cathode material in the form of LiF/Fe composite (discharged state of FeF_3). LiF/Fe composite can be prepared through various routes, such as combinatorial sputtering [20], ball milling [21] and electrospinning followed by thermal decomposition [22]. Prakash et al. [23] prepared LiF/Fe/C composite by decomposing ferrocene in the presence of nano sized LiF. The composite showed a high reversible capacity of ~270 mA h g^{-1} (w.r.t. the active mass LiF/Fe) at 20.83 mA g^{-1} in the voltage window of 0.5–4.3 V, being stable for at least 200 cycles. Li et al. [21] prepared LiF/Fe composite by adding TiN and graphite as conducting reagents and showed 568 mA h g^{-1} at 20 mA g^{-1} current density. They calculated the capacity w.r.t. the active material which is only 50% of the total mass loading.

In this present investigation, we prepared LiF/Fe nanocomposites with different amounts of V_2O_5 as conducting additive by a simple ball milling method. The nanocomposites were characterized by XRD, SEM, TEM techniques. LiF/Fe ball milled nanocomposite without V_2O_5 showed poor Li cycling performance. With the addition of V_2O_5, the electrochemical performance of LiF/Fe nanocomposites was improved due to an increase in electronic as well as in ionic conductivities. The nanocomposite with 15 wt.% of V_2O_5 ball milled for 30 h showed better Li cycling performance compared to the nanocomposites with 0, 10 and 20 wt.% of V_2O_5. Further, we noticed that the LiF/Fe/V_2O_5 (15 wt.%, 20 h ball milled) nanocomposite when heat treated showed improved cycling stability compared to the as prepared nanocomposite. Cyclic voltammetry (CV), electrochemical impedance spectroscopy (EIS) and ex-situ TEM at the charged state (4.3 V) after 30 cycles were carried out on the LiF/Fe/V_2O_5 (15 wt.%, 30 h ball milled) nanocomposite to understand the reaction mechanism.

2. Experimental

For the preparation of LiF/Fe/V_2O_5 nanocomposites with different gravimetric content of V_2O_5, calculated amount of LiF, Fe and V_2O_5 were weighed maintaining LiF to Fe as 3:1 mol ratio inside an Ar filled glove box (MBraun, Germany), where H_2O and O_2 levels were maintained at <1 ppm (All the operations were carried out inside an Ar filled glove box unless otherwise stated). The materials were transferred to tungsten carbide (WC) container. WC balls were used for milling with ball to powder mass ratio of 60:1. Ball milling was carried out for different milling times (30, 20 and 10 h), in steps of 20 min with 10 min relaxation time at the rotation speed of 400 rpm, to avoid a significant rise in temperature in the vial. After milling, vials were opened and the material was collected for characterizations. For some samples, as prepared LiF/Fe/V_2O_5 (15 wt.%; 20 h ball milled) nanocomposite was heat treated at 300 °C for 20 min in a tube furnace under flowing Ar gas. The furnace was heated at 5 °C per min and cooled naturally to room temperature.

The materials were characterized by powder X-ray diffraction (XRD) using an STOE Stadi P diffractometer equipped with a Dectris Mythen 1 K linear silicon strip detector and Ge (111) double crystal monochromator (Mo $K_{\alpha 1}$-radiation, λ = 0.7093 Å). XRD patterns were recorded at room temperature (25 °C) in a 2θ range between 10 to 70°. Powder samples were ground to fine particles and filled in a capillary tube and sealed to prevent oxidation of nanocrystalline Fe present in the composites. The XRD patterns were analyzed by using the TOPAS software package (A. A. Coelho, TOPAS Academic V4.1 (2007), Coelho Software, Brisbane). Morphology and the microstructure of the nanocomposites were studied by scanning electron microscopy (SEM) using a Leo-1530 instrument. Transmission electron microscopy (TEM) characterization of the as prepared nanocomposite was carried out using an aberration corrected FEI Titan 80–300 operated at 80 kV equipped with a Gatan imaging filter (Tridiem 863). For TEM measurement, samples were

prepared by dispersing a small amount of powder directly onto holey carbon Au grids (Quantifoil GmbH). The grids were placed on a Gatan vacuum transfer holder and transferred. The TEM holder was reopened inside the TEM, minimizing exposure to the atmosphere. For ex-situ TEM measurement, electrodes were charged to selective voltage. The cell was opened and a little amount of sample was loaded onto the Au grid and a similar procedure was followed as stated above for the TEM measurements.

Electrodes fabrication was carried out using the active material, carbon black (Alfa Aesar) and PVDF binder (Alfa Aesar) in the weight ratio 70:15:15 using *N*-methyl-2-pyrrolidinone (NMP) as the solvent for the binder. The thick slurry prepared from the above mentioned compositions was manually coated onto surface cleaned stainless steel discs, used as current collectors (12 mm diameter) with the help of flat stainless steel spatula and dried at 80 °C overnight in order to evaporate the NMP. Li metal (Goodfellow) was used as the counter electrode. 1 M $LiPF_6$ in ethylene carbonate (EC) and dimethyl carbonate (DMC) (volume ratio of 1:1) (LP30/Merck) was used as the electrolyte and glass microfiber filter (GF/F) (Whatman Int. Ltd., Maidstone, England) as the separator. Two electrode Swagelok cells were fabricated using LiF/Fe/V_2O_5 composite electrodes as cathodes and Li metal as anode. More details on the cell fabrication are described elsewhere [24,25]. The fabricated cells were rested for 5 h before measurement to ensure complete penetration of electrolyte into the active material. The active mass loading in the Swagelok type cell was ~6–7 mg. The mass loading per cm^2 was calculated to be ~6.2 mg cm^{-2}. Galvanostatic charge/discharge cycling was carried out in the voltage range of 1.3–4.3 V at room temperature using multichannel battery tester Arbin BT 2000. Cyclic voltammetry (CV) at constant potential sweep was carried out using an Autolab potentiostat. Electrochemical impedance measurement (EIS) was carried out with a Biologic VMP3 potentiostat at room temperature (RT). The frequency range was varied from 1.0 MHz to 3 mHz with an AC signal amplitude of 10 mV. Data were collected and analyzed using *Z* plot and Z view software (Scribner Associates Inc.; 2.2 version) to obtain the Nyquist plots ($-Z''$ vs. Z).

3. Results and discussion

LiF/Fe/V_2O_5 nanocomposites, with x wt.% of V_2O_5 ($x = 0$, 10, 15 and 20) were prepared by using high energy ball milling from micron sized LiF, Fe (3:1 mol ratio) and V_2O_5 powder. High energy ball milling is necessary in order to reduce the particle size of the components to nanoscale regime to obtain improvements in the electrochemical cycling performance due to improved transport properties for Li ions [26]. Here, we can mention that these systems were studied due to their high specific capacities and high energy densities. The theoretical capacity of these nanocomposites are: 580, 570 and 560 mA h g^{-1} for LiF/Fe/V_2O_5 (10 wt.%), LiF/Fe/V_2O_5 (15 wt.%) and LiF/Fe/V_2O_5 (20 wt.%), respectively. The experimental energy density obtained are: 420, 1250 and 610 Wh kg^{-1} for LiF/Fe/V_2O_5 (10 wt.%), LiF/Fe/V_2O_5 (15 wt.%) and LiF/Fe/V_2O_5 (20 wt.%), respectively. X-ray diffraction (XRD) pattern of the as prepared LiF/Fe/V_2O_5 (15 wt.%, 30 h ball milled) nanocomposite is shown in Fig. 1. It shows characteristic peaks for cubic α-Fe (JCPDS: 00-006-0696) and LiF (JCPDS:00-004-0857) and no peaks correspond to V_2O_5 are seen possibly due to amorphisation or phase transformation during ball milling. The impurity peaks are assigned to WC (JCPDS: 01-072-0097) from the grinding media. It is seen that the peaks are broadened, indicating the reduction in particle size during high energy ball milling.

Morphology and microstructure of the as prepared LiF/Fe/V_2O_5 (15 wt.%, 30 h ball milled) nanocomposite were characterized by SEM and TEM. SEM images of the as prepared LiF/Fe/V_2O_5 (15 wt.%, 30 h ball milled) nanocomposite are shown in Fig. 2a and b. The as prepared nanocomposite was composed of agglomerated nanoparticles. Due to high energy ball milling the particle size of the composite ranged from a few nanometers to a few hundred nanometers. Bright-field TEM images of the as prepared LiF/Fe/

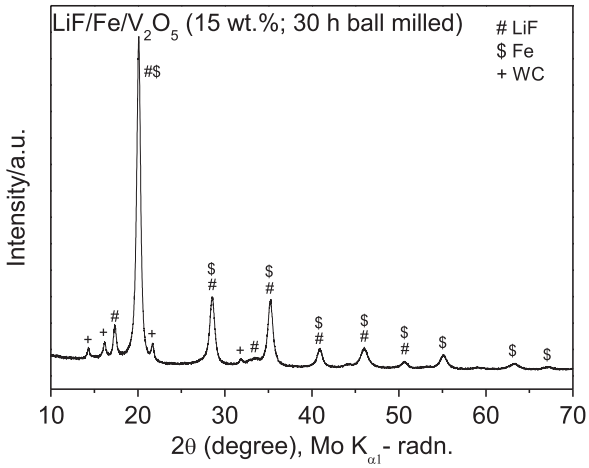

Fig. 1. X-ray diffraction pattern of LiF/Fe/V_2O_5 (15 wt.%; 30 h ball milled) nanocomposite prepared by high energy ball milling.

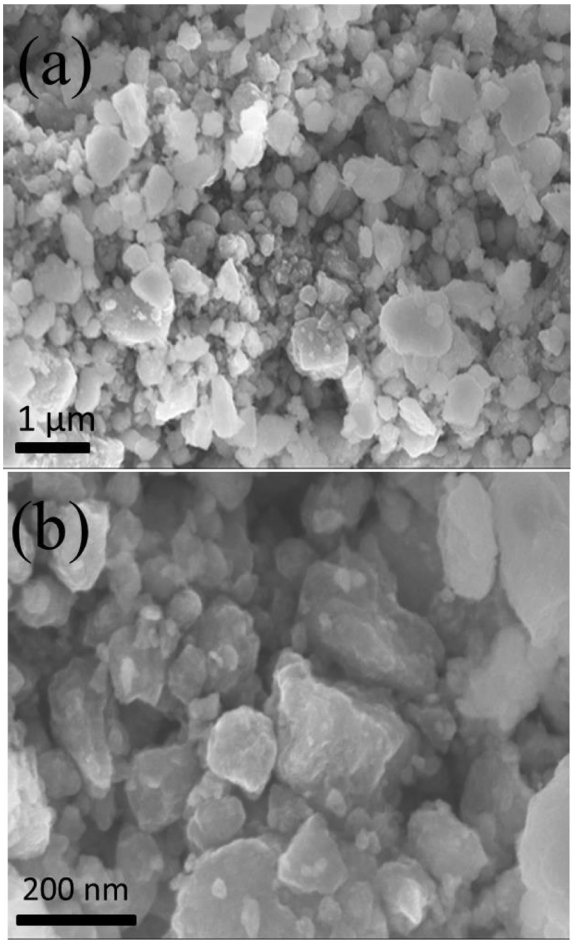

Fig. 2. SEM micrograph of LiF/Fe/V_2O_5 (15 wt.%; 30 h ball milled) nanocomposite prepared by high energy ball milling.

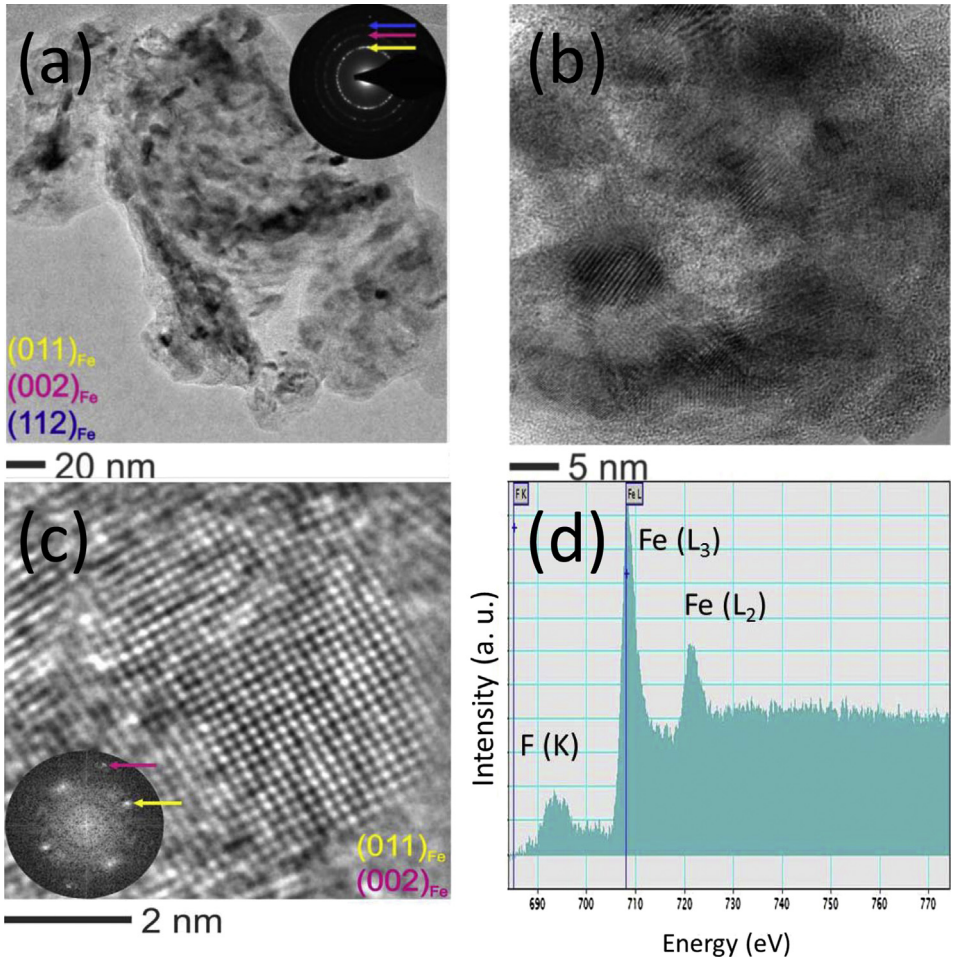

Fig. 3. TEM characterization of LiF/Fe/V_2O_5 (15 wt.%; 30 h ball milled) nanocomposite prepared by high energy ball milling. (a) TEM image at low magnification (Inset: SAED pattern); (b, c) HRTEM micrograph; (d) EELS spectrum.

V_2O_5 (15 wt.%, 30 h ball milled) nanocomposite are shown in Fig. 3. TEM image at low magnification (Fig. 3a) shows the agglomeration of particles with irregular shape. Selected area electron diffraction (SAED) pattern of the as prepared LiF/Fe/V_2O_5 (15 wt.%, 30 h ball milled) taken from same area (inset picture) indicates a polycrystalline material with reflections corresponding to α-Fe. The spacings observed in the fast Fourier transformation (FFT) of the HRTEM image (Fig. 3c) correspond to the $(011)_{\alpha\text{-Fe}}$ and $(002)_{\alpha\text{-Fe}}$ lattice planes. Electron energy loss spectroscopy (EELS) depicts the Fe L-edge (L_2 and L_3) and the F K-edge (Fig. 3d). These edges correspond to the presence of Fe and F in the nanocomposite, respectively [27,28].

Li cycling performance of LiF/Fe/V_2O_5 (15 wt.%, 30 h ball milled) nanocomposite was carried out by galvanostatic cycling in the voltage range of 1.3–4.3 V at 20 mA g^{-1} up to 50 cycles. The corresponding voltage vs. capacity profiles are shown in Fig. 4. Specific capacity was calculated with respect to the total weight of the active material (i.e. LiF/Fe/V_2O_5). Initially, the cell was charged from its open circuit voltage (OCV; 2.58 V) to a fully charged state; i.e. 4.3 V. During the first charge, the nanocomposite showed a continuous increase of voltage until ~3.2 V, followed by a large plateau at ~3.5 V. This voltage plateau is attributed to the reaction of LiF/Fe to form FeF_2 (Eq. (4)) (Fig. S1; Supplementary information) [16,29].

$$2LiF + Fe \leftrightarrow FeF_2 + 2Li^+ + 2e^- \quad (4)$$

LiF is decomposed to form Li^+ and F^- ions and the freshly formed F^- ion combined with Fe to form FeF_2. It can be seen that the total charge specific capacity observed at the end of ~4.3 V was ~420 (±5) mA h g^{-1}. During the subsequent discharge reaction, the voltage vs. capacity profile shows well defined two stage reaction in

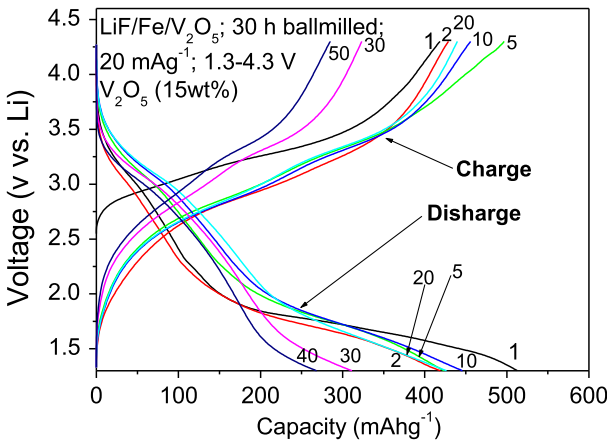

Fig. 4. Galvanostatic charge–discharge profile of LiF/Fe/V_2O_5 (15 wt.%; 30 h ball milled) nanocomposite prepared by high energy ball milling. Current density: 20 mA g^{-1}; voltage range: 1.3–4.3 V. Numbers show cycle numbers.

the voltage region of ~3.5–2.25 V and ~2.0–1.3 V. These voltage plateaus correspond to the insertion of Li ions, followed by conversion reaction to form LiF/Fe^0 [7–9,16,23]. At the end of first discharge, the observed total specific capacity was ~510 (±5) mA h g^{-1}. The subsequent discharge and charge profiles from 2–50 cycles qualitatively resemble to that of the first cycle profiles except for the gradual decrease in the capacity values till 50th cycle. At the end of 50th cycle, the LiF/Fe/V_2O_5 (15 wt.%, 30 h ball milled) nanocomposite showed a reversible capacity of ~270 (±5) mA h g^{-1}.

Fig. 5a and b shows the capacity vs. cycle number plots of the LiF/Fe/V_2O_5 nanocomposites with different V_2O_5 content and ball milling times up to 50 cycles. For LiF/Fe nanocomposites with *x* wt.% of V_2O_5 ($x = 0, 10, 15$ and 20), the capacity vs. cycle number plots are shown in Fig. 5a. LiF/Fe composite without V_2O_5 showed a high initial capacity, but a drastic capacity fading was noticed upon cycling. It showed a first charge capacity of ~400 (±5) mA h g^{-1}, whereas the first discharge capacity was ~375 (±5) mA h g^{-1}. After 20th cycle, the reversible capacity observed was almost negligible compared to that of the first cycle. The reason for such drastic decay may be attributed to the poor electrical conductivity of the fluorides. When V_2O_5 was added to LiF/Fe, the electrochemical performance was drastically improved and better capacity retention was observed at higher cycle number. LiF/Fe composite with 15 wt.% V_2O_5 showed the best performance with a high first cycle charge capacity of ~420 (±5) mA h g^{-1}, while the first discharge capacity was 510 (±5) mA h g^{-1}. It was observed that the reversible capacity initially dropped till 3rd cycle, followed by an increase until 16th cycle and thereafter a gradual fading was observed till 50th cycle. At the end of 50th cycle, the reversible capacity was ~270 (±5) mA h g^{-1}, which is 53% of the first cycle discharge capacity. The Coulombic efficiency was improved upon cycling and reached almost 95% at the end of 50th cycle. The Coulombic efficiency was calculated for 2nd cycle onwards. LiF/Fe nanocomposites with 10 and 20 wt.% V_2O_5 showed similar cycling performance, but lower capacity values were observed in both cases. At the end of 50th cycle, the observed reversible capacities were 170 and 70 (±5) mA h g^{-1} for 20 and 10 wt.% V_2O_5, respectively. Enhanced Li cycling behavior can be inferred from the voltage vs. capacity profiles (Fig. S2; Supplementary information), as the voltage plateau is prominent with nanocomposites consisting of 15 wt.% V_2O_5 compared to others. This observation can be attributed to the improved ionic and electronic conductivities of the nanocomposite at the optimized composition (Fig. S3; Supplementary information). Initially, the composite with 15 wt.% V_2O_5 showed notable difference in the charge and discharge capacity and also high fading rate (Fig. 5a). Although, 20 wt.% V_2O_5 composite showed lower specific capacity than the composite with 15 wt.% V_2O_5, the capacity fading rate is less in the former, which is possibly due to presence of higher amount of V_2O_5 (Fig. 5a). The 10 wt.% V_2O_5 showed very low initial capacity and moderate capacity fading.

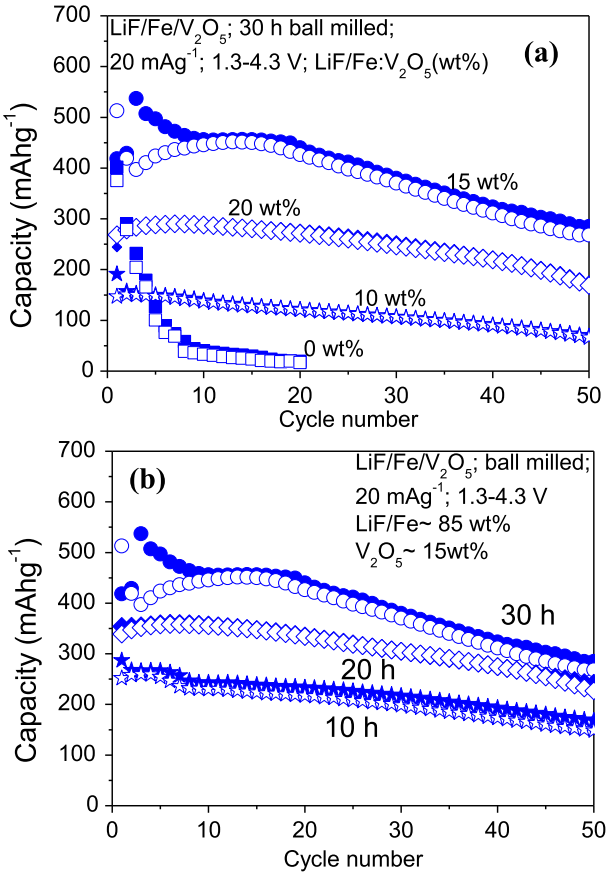

Fig. 5. Specific capacity vs. cycle number plot of LiF/Fe/V_2O_5 nanocomposite prepared by high energy ball milling: (a) with varying V_2O_5 content (in wt.%); (b) with varying ball milling time. Current density: 20 mA g^{-1}; voltage range: 1.3–4.3 V. Open symbol: discharge capacity; closed symbol: charge capacity.

Badway et al. [17] showed an improved electrochemical performance of CuF_2 in the presence of mixed conducting matrix such as MoO_3, VO_2, V_2O_5. In contrast, CuF_2 did not show good cycling performance when cycled in the presence of CuO or NiO. They explained that CuO and NiO did not show Li ion intercalation which would be needed for very good ionic conductivity in addition to their excellent electrical (or electronic) conductivity. Similar to their findings, we have noticed poor cycling performance of LiF/Fe in the presence of V_2O_3 (Figure not shown). While V_2O_3 shows very good electrical conductivity [30], it does not show Li ion intercalation. Hence, it is necessary to use a suitable matrix which offers both Li ion transport and good electrical conductivity. The orthorhombic V_2O_5 has an open structure for Li ion intercalation during cycling [31] and it is also a semiconductor [32]. Thus combination of these two properties makes V_2O_5 a true mixed conductor. The presence of V_2O_5 supplements ionic conductivity before and during the conversion reaction of LiF/Fe ↔ FeF_2 (eqn. (4)). Further, the energetic levels of V_2O_5 i.e. intercalation/de-intercalation potentials are in the range of the conversion potential of LiF/Fe [33], facilitating Li cycling performance in LiF/Fe nanocomposite during cycling similar to CuF_2 studied by Badway et al. [17].

The poor kinetics is a major drawback in case of conversion reaction based electrode materials. Slow transport of Li ions and/or electrons limits the kinetics, which can be improved by reducing the diffusion distance by reducing the effective size of the particles to nanoscale [26]. Hence, LiF/Fe/V_2O_5 (15 wt.%) nanocomposite has been subjected to ball milling with different milling times to study the influence of milling time on its electrochemical performance. Fig. 5b shows the capacity vs. cycle number plot for LiF/Fe/V_2O_5 (15 wt.%) nanocomposites with various ball milling times (10, 20 and 30 h). It is seen that the ball milling time is directly proportional to the enhancement in the electrochemical performance of the nanocomposites (Fig. 5b). LiF/Fe nanocomposite ball milled for 30 h showed better cycling performance compared to 10 and 20 h. This is possibly due to reduction of grain size which decreased the effective diffusion length for Li ions and hence improved the Li ion kinetics [26]. Also change in morphology with higher ball milling time is another possible reason for improved Li cycling (which is not clear from SEM due to strong agglomeration). As a result, the Li cycling performance was improved. The effect of milling time on the electrochemical performance of LiF/Fe/V_2O_5 is clearly noticed

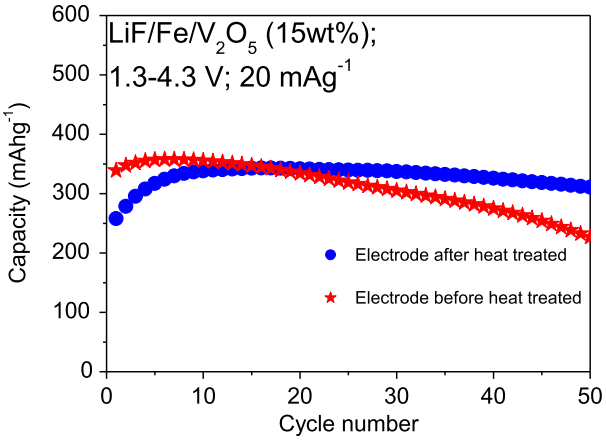

Fig. 6. Specific capacity vs. cycle number plot of LiF/Fe/V_2O_5 (15 wt.%, 20 h ball milled) nanocomposite before and after heat treatment. Current density: 20 mA g^{-1}; voltage range: 1.3–4.3 V. Only discharge capacities are shown.

from Fig. 5b. They showed high initial capacity value, but resulted in capacity fading when cycled for longer time. At the end of 50th cycle, the observed reversible capacities were ~270, 230 and 150 (±5) mA h g^{-1} for 30, 20 and 10 h ball milled nanocomposites, respectively.

Interestingly, an improved Li cyclability was observed for the LiF/Fe/V_2O_5 (15 wt.%, 20 h ball milled) nanocomposite when heat treated compared to as prepared material and the result is shown in Fig. 6. The ball milled nanocomposite after heat treatment was named as HT-LiF/Fe/V_2O_5. Recently, Yabuuchi et al. [34] showed an improved Li cycling performance of ball milled FeF_3/C composite after heat treatment. They explained that better Li cycling performance was noticed for heat treated ball milled FeF_3/C composite due to suppress in strain. It is reasonable to extend the same explanation for HT-LiF/Fe/V_2O_5 nanocomposite. It showed an initial capacity which was below that of the as prepared nanocomposite. With increase in cycle number, the capacity was increased to higher value and became stable after 10 cycles. A high and stable capacity of ~310 (±5) mA h g^{-1} was noticed at the end of 50th cycle, whereas only ~230 (±5) mA h g^{-1} was noticed for as prepared nanocomposite. Slow capacity degradation was observed for HT-LiF/Fe/V_2O_5 nanocomposite when cycled beyond 50 cycles.

The differential capacity (dQ/dV) plots for the 2nd, 10th and 50th cycle of LiF/Fe/V_2O_5 (15 wt.%, 20 h ball milled) nanocomposite before and after heating are compared and shown in Fig. 7. As prepared nanocomposite showed the voltage peaks at ~2.89, ~3.2 V during charge and ~3.07, ~2.24 and ~1.87 V during discharge (Fig. 7a), indicating that the phase transition occurred in several stages. Heat treated nanocomposite also showed similar voltage peaks with slight shifts in voltage positions (Fig. 7c). The voltage peaks for both cases are identical till 10th cycle (Fig. 7b and d). However, a major difference for both samples was noticed at 50th cycle where a clear shift of the voltage peak (~1.87 V) during discharge was observed in case with as prepared nanocomposite. Here, an increase in polarization was noticed with increasing in cycle number. In contrast, the heat treated nanocomposite did not show significant increase in polarization at higher cycle numbers.

To investigate the redox potential and the reaction mechanism, cyclic voltammetry (CV) studies were carried out for the LiF/Fe/V_2O_5 (15 wt.%, 30 h ball milled) nanocomposite in the voltage range 1.3–4.3 V at the slow scan rate 100 μV s^{-1} up to 5 cycles (Fig. 8). Initially, the cell was charged from its OCV (~2.6 V) to 4.3 V. In the first cycle, it showed couple of oxidation peaks centered at ~3.0 and ~3.35 V. These peaks correspond to the extraction of Li ions from the nanocomposite and formation of FeF_2 from LiF/Fe^0 through the conversion reaction (Eq. (4)) (Fig. S1; Supplementary information) [16,23,29]. The corresponding reduction peaks were seen at ~3.0 and ~1.7 V due to insertion of Li ions to FeF_2, followed by conversion

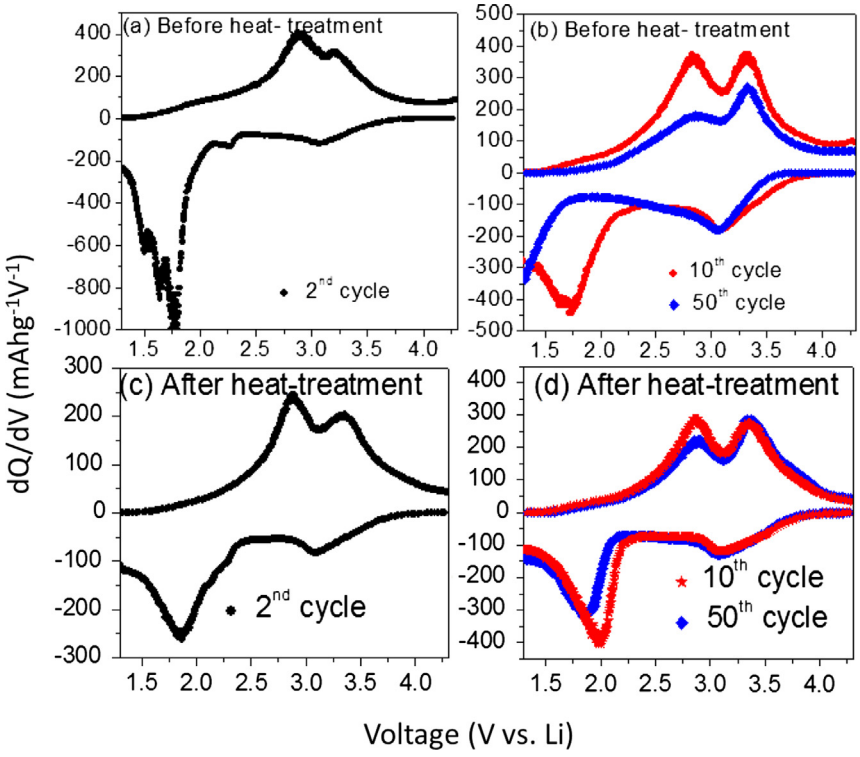

Fig. 7. Differential capacity plot of LiF/Fe/V_2O_5 (15 wt.%, 20 h ball milled) nanocomposite prepared by high energy ball milling (a, b) as prepared; (c, d) after heat treatment.

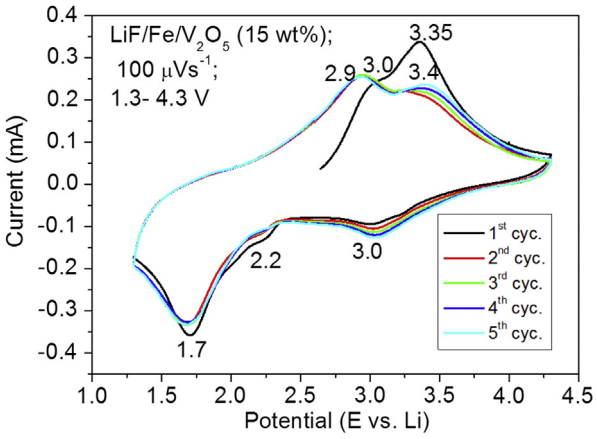

Fig. 8. Cyclic voltammogram of LiF/Fe/V_2O_5 (15 wt.%, 30 h ball milled) nanocomposite prepared by high energy ball milling. Scan rate: 100 μV s^{-1}; voltage range: 1.3–4.3 V.

to LiF/Fe^0 [16,29]. We noticed a shoulder peak at ~2.2 V during reduction process, which is possibly from vanadium oxide (amorphous) present in the nanocomposite [33]. Further oxidation/reduction scans showed similar profile and almost overlapping each other indicating a well reversible electrochemical cyclability of LiF/Fe/V_2O_5 (15 wt.%, 30 h ball milled) nanocomposite. An increase in the area under *I*/*V* curve with increase in cycle number was noticed, indicating an increase in capacity during cycling. Similar behavior was found for galvanostatic cycling for initial few cycles, as mentioned earlier (Fig. 5).

TEM measurement on the LiF/Fe/V_2O_5 (15 wt.%, 30 h ball milled) nanocomposite charged to 4.3 V at a current density of 20 mA g^{-1} at the end of the 30th cycle was carried out and are shown in Fig. 9. TEM image after charging (Fig. 9a) reveals the homogeneous distribution of electrochemically formed iron fluoride nanoparticles in the vanadium oxide. EELS shows the F K-edge and Fe L-edge confirming the presence of F and Fe in the nanocomposite (Inset). In addition, the scanning transmission electron microscopy (STEM)-EDX elemental maps (Fig. 9b) confirm the distribution of Fe and F in the V and O. The formation of FeF_2 was confirmed from ex-situ XRD (Fig. S1; Supplementary information).

Electrochemical impedance spectroscopy (EIS) measurements on electrode materials at different charge and discharge voltages give information on the factors responsible for the overall impedance during the Li cycling [35–39]. The experimental data obtained were analyzed in more detail in order to understand the Li ion reaction mechanism during charge–discharge process. EIS measurements were carried out on the cell comprising of LiF/Fe/V_2O_5 (15 wt.%, 30 h ball milled) (and LiF/Fe for comparison) as the working electrode vs. Li during the first charge–discharge cycle, at selected voltages at a current density 20 mA g^{-1}. The chosen potential regions are based on Li^+ extraction or insertion during charge and discharge process. Results are presented as Nyquist plots ($-Z''$ vs. Z), where Z and Z'' refer to the real and imaginary parts of cell impedance, respectively (Fig. 10b–e). The spectra were fitted with an equivalent electrical circuit using serial and parallel combinations of resistances (R), CPEs (constant phase element), W_s (Warburg impedance) and intercalation capacitance (C_i). Equivalent circuit used for data fitting is shown in Fig. 10f.

The observed total impedance is made up of contributions from different factors such as electrolyte resistances (R_e), impedance due to surface film (R_{sf}), charge transfer (R_{ct}) resistance and the associated surface film (CPE_{sf}) and double layer (CPE_{dl}) capacitance and Warburg impedance (W_s). CPEs were used instead of pure capacitor, since the Nyquist plots showed depressed semicircles, which

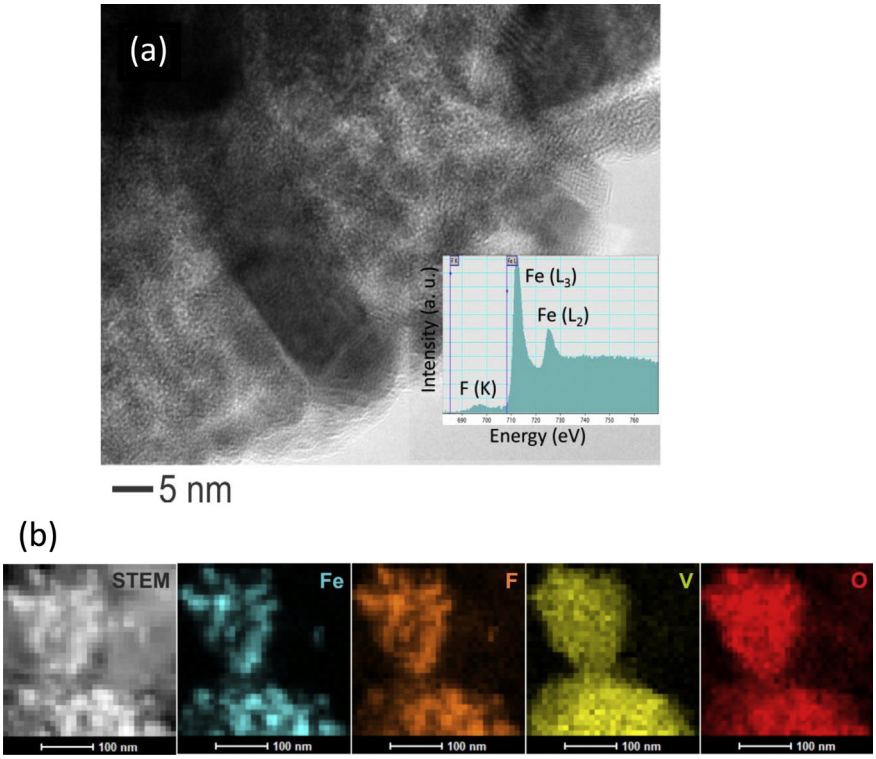

Fig. 9. Ex-situ TEM characterization of cycled LiF/Fe/V_2O_5 (15 wt.%; 30 h ball milled) nanocomposite at 4.3 V after 30 cycles. (a) TEM image; EELS showing the presence of Fe and F in the charged state (4.3 V) after 30 cycles (Inset). (b) STEM-HAADF image and the corresponding EDX elemental maps.

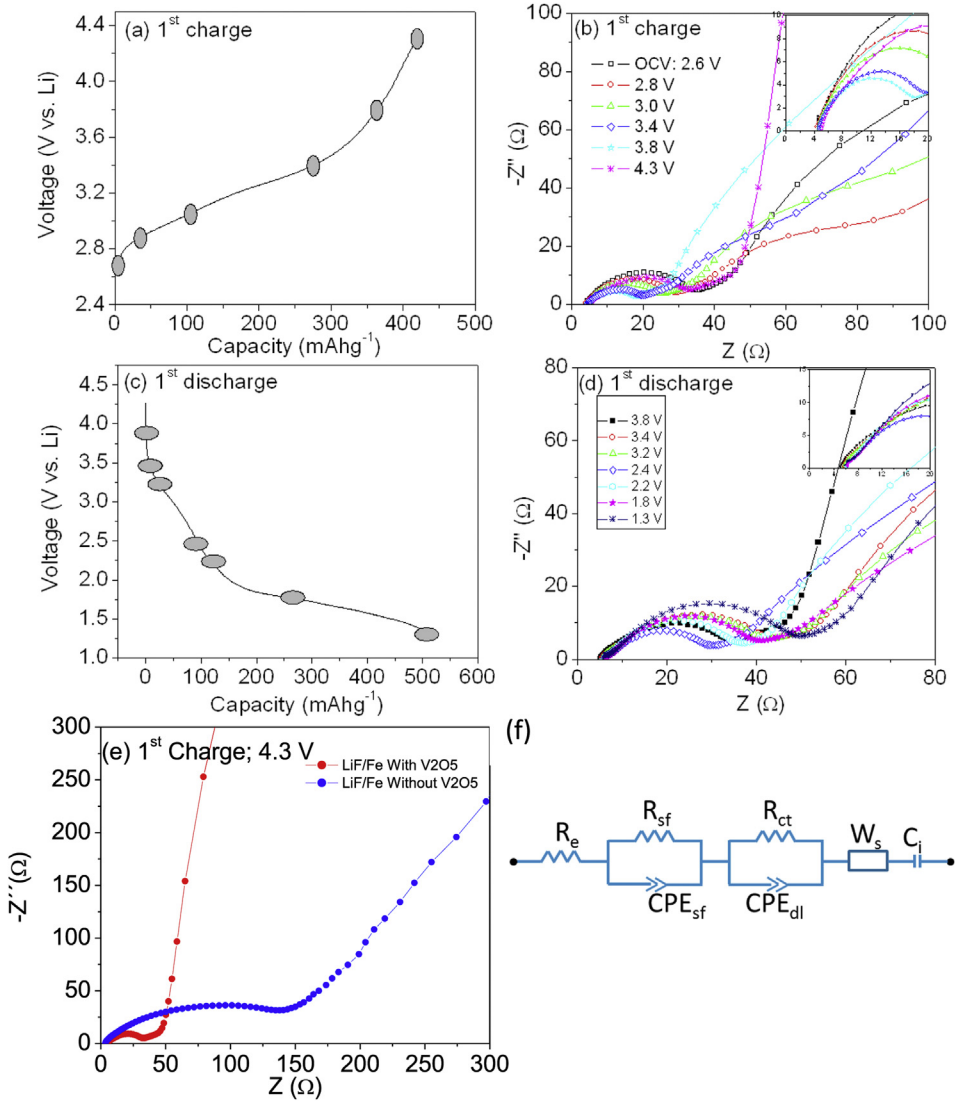

Fig. 10. LiF/Fe/V_2O_5 (15 wt.%; 30 h ball milled) nanocomposite: (a) voltage vs. capacity profile during 1st charge; (b) Nyquist plots ($-Z''$ vs. Z) at selected voltages during 1st charge; (c) voltage vs. capacity profile during 1st discharge; (d) Nyquist plots ($-Z''$ vs. Z) at selected voltages during 1st discharge; (e) comparison of cell impedance of LiF/Fe nanocomposite with and without V_2O_5; (f) equivalent circuit used to fit the experimental data.

indicate a deviation from the ideal behavior. Impedance due to constant phase element is $Z_{CPE} = 1/[C(j\omega)^{\alpha}]$ where $j = \sqrt{-1}$, ω is the angular frequency, C is the capacitance and α is a constant. The value of α varies in the range $0 < \alpha < 1$, which gives the degree of distortion from the pure capacitor behavior ($\alpha = 1$ for pure capacitor). The extracted impedance parameters are given in Table 1. Electrolyte resistance (R_e) which is due to the Li ion transport in electrolyte was found to be ~5 Ω and is similar in all cases. At OCV (~2.6 V), the impedance spectra showed a well-defined semicircle at high frequency region and an undeveloped arc type at low frequency region (Fig. 10b). Impedance at high and medium frequency region is the contribution from the formation of SEI and the charge transfer across the electrode/electrolyte interface [35,40]. When the cell was charged from OCV to 4.3 V, the overall impedance $R_{(sf\,+\,ct)}$ decreased from 31 (±2) Ω to 12 (±2) Ω (at 3.8 V). At fully charged state (4.3 V), the $R_{(sf\,+\,ct)}$ value increased slightly to 18 (±2) Ω (Table 1). At OCV, the observed high impedance value is due to the presence of highly insulating LiF in the nanocomposite which is both electronic and ionic insulator. During the charging process, the overall impedance shifts from ~2.6 V to ~3.0 V. In this potential range, partial oxidation of Fe^0 to Fe^{2+} occurs through conversion reaction. With further delithiation, a large decrease in overall impedance was noticed in the voltage range from ~3.0 V to ~3.8 V indicating fully conversion of LiF/Fe to FeF_2 (Eq. (4)) [23,29]. During discharge process (where Li ion insertion to

Table 1
Impedance parameter of LiF/Fe/V_2O_5 (15 wt.%, 30 h ball milled) nanocomposite during the 1st charge–discharge cycle at various voltages. The open circuit voltage (OCV) was ~2.6 V.

	Cell voltages in volt (V)	$R_{(sf\,+\,ct)}$ (±2) in ohm (Ω)
1st charge	OCV (2.6)	31
	2.8	26
	3.0	22
	3.4	14
	3.8	12
	4.3	18
1st discharge	3.8	18
	3.4	26
	3.2	25
	2.4	21
	2.2	19
	1.8	22
	1.3	30

the electrode occurs), the impedance spectra (Fig. 10d) showed initial increase in overall impedance value ($R_{(sf+ct)}$) from 18 to 25 (±2) Ω when discharged to 3.2 V, followed by decrease till 2.2 V. The overall impedance value ($R_{(sf+ct)}$) observed at 2.2 V is 19 (±2) Ω. It is expected that the overall impedance value should increase due to the formation of LiF (which is highly insulating in nature) through conversion reaction [35]. The inverse trend in the voltage range 3.2 to 2.2 V is possibly due to the presence of amorphous vanadium oxide, which shows Li intercalation in this voltage range [33] and forms intermediate lithiated vanadium oxide of higher conductivity and hence possibly reduced overall impedance. When discharged from 2.2 V to 1.3 V, the increase in overall impedance was observed due to complete formation of LiF [35]. We have also compared the overall impedance observed for LiF/Fe nanocomposite with and without addition of V_2O_5 during ball milling (Fig. 10e). LiF/Fe composite with V_2O_5 showed lower impedance value compared to composite without V_2O_5, indicating the increase in conductivity of the composite materials and hence better electrochemical performance was observed.

4. Conclusions

LiF/Fe nanocomposites with V_2O_5 (at different wt.%) as conductive additive were prepared by high energy ball milling with different milling times. The nanocomposites were characterized by XRD, SEM and TEM which indicate nano-sized Fe and LiF distributed in the vanadium oxide. Li cycling behavior was investigated by using galvanostatic cycling and cyclic voltammetry (CV) techniques. The results show that the addition of V_2O_5 dramatically improves the performance of LiF/Fe nanocomposite by improving electronic as well as ionic conductivity. LiF/Fe/V_2O_5 (15 wt.%, 30 h ball milled) showed the best Li cycling performance among various compositions. A high first cycle discharge capacity of ~510 (±5) mA h g^{-1} was found followed by a sharp decay and a gradual increase in capacity up to 16th cycle with a subsequent slow capacity degradation till 50th cycle. The capacity observed at the end of 50th cycle was ~270 (±5) mA h g^{-1}. LiF/Fe/V_2O_5 (15 wt.%, 20 h ball milled) nanocomposite subjected to heat treatment showed an improved cycling stability against the as prepared nanocomposite and a high reversible capacity of ~310 (±5) mA h g^{-1} was noticed at the end of 50th cycle. The average charge–discharge potentials observed from the CV were ~2.9 and ~1.7 V, respectively. TEM studies of cycled electrode charged to 4.3 V after 30th cycle showed presence of Fe and F in the composite and distributed homogeneously. FeF_2 formation through conversion reaction was confirmed from ex-situ XRD measurement. Electrochemical impedance spectroscopy (EIS) measurement at selected voltages during charge and discharge process of first cycle supported the proposed reaction mechanism.

Acknowledgment

Support by Karlsruhe Nano Micro Facility (KNMF) is gratefully acknowledged.

Appendix A. Supplementary data

Supplementary data related to this article can be found at http://dx.doi.org/10.1016/j.jpowsour.2014.05.063.

References

[1] M.S. Whittingham, Chem. Rev. 104 (2004) 4271.
[2] V. Etacheri, R. Marom, R. Elazari, G. Salitra, D. Aurbach, Energy Environ. Sci. 4 (2011) 3243.
[3] M. Jo, S. Jeong, J. Cho, Electrochem. Commun. 12 (2010) 992.
[4] M. Okubo, E. Hosono, J. Kim, M. Enomoto, N. Kojima, T. Kudo, H. Zhou, I. Honma, J. Am. Chem. Soc. 129 (2007) 7444.
[5] L. Wang, X. He, W. Sun, J. Wang, Y. Li, S. Fan, Nano Lett. 12 (2012) 5632.
[6] C.R. Sides, F. Croce, V.Y. Young, C.R. Martin, B. Scrosati, Electrochem. Solid-State Lett. 8 (2005) A484.
[7] D. Ma, Z. Cao, H. Wang, X. Huang, L. Wang, X. Zhang, Energy Environ. Sci. 5 (2012) 8538.
[8] L. Liu, M. Zhou, L. Yi, H. Guo, J. Tan, H. Shu, X. Yang, Z. Yang, X. Wang, J. Mater. Chem. 22 (2012) 17539.
[9] G.G. Amatucci, N. Pereira, J. Fluorine Chem. 128 (2007) 243.
[10] M. Zhou, L. Zhao, T. Doi, S. Okada, J. Yamaki, J. Power Sources 195 (2010) 4952.
[11] T. Li, L. Li, Y.L. Cao, X.P. Ai, H.X. Yang, J. Phys. Chem. C 114 (2010) 3190.
[12] H. Arai, S. Okada, Y. Sakurai, J. Yamaki, J. Power Sources 68 (1997) 716.
[13] F. Badway, N. Pereira, F. Cosandey, G.G. Amatucci, J. Electrochem. Soc. 150 (2003) A1209.
[14] X. Zhao, C.M. Hayner, M.C. Kung, H.H. Kung, Chem. Commun. 48 (2012) 9909.
[15] J. Liu, Y. Wan, W. Liu, Z. Ma, S. Ji, J. Wang, Y. Zhou, P. Hodgson, Y. Li, J. Mater. Chem. A 1 (2013) 1969.
[16] M.A. Reddy, B. Breitung, V.S.K. Chakravadhanula, C. Wall, M. Engel, C. Kübel, A.K. Powell, H. Hahn, M. Fichtner, Adv. Energy Mater. 3 (2013) 308.
[17] F. Badway, A.N. Mansour, N. Pereira, J.F. Al-Sharab, F. Cosandey, I. Plitz, G.G. Amatucci, Chem. Mater. 19 (2007) 4129.
[18] W. Wu, Y. Wang, X. Wang, Q. Chen, X. Wang, S. Yang, X. Liu, J. Guo, Z. Yang, J. Alloys Compd. 486 (2009) 93.
[19] W. Wu, X. Wang, X. Wang, S. Yang, X. Liu, Q. Chen, Mater. Lett. 63 (2009) 1788.
[20] P. Liao, B.L. MacDonald, R.A. Dunlap, J.R. Dahn, Chem. Mater. 20 (2008) 454.
[21] T. Li, Z.X. Chen, X.P. Ai, Y.L. Cao, H.X. Yang, J. Power Sources 217 (2012) 54.
[22] S. Zhang, Y. Lu, G. Xu, Y. Li, X. Zhang, J. Phys. D Appl. Phys. 45 (2012) 395301.
[23] R. Prakash, A.K. Mishra, A. Roth, C. Kübel, T. Scherer, M. Ghafari, H. Hahn, M. Fichtner, J. Mater. Chem. 20 (2010) 1871.
[24] C. Wall, R. Prakash, C. Kübel, H. Hahn, M. Fichtner, J. Alloys Compd. 530 (2012) 121.
[25] S. Ren, R. Prakash, D. Wang, V.S.K. Chakravadhanula, M. Fichtner, ChemSusChem 5 (2012) 1397.
[26] P.G. Bruce, B. Scrosati, J.-M. Tarascon, Angew. Chem. Int. Ed. 47 (2008) 2930.
[27] R. Che, C. Liang, H. Shi, X. Zhou, X. Yang, Nanotechnology 18 (2007) 355705.
[28] F. Cosandey, J.F. Al-Sharab, F. Badway, G.G. Amatucci, P. Stadelmann, Microsc. Microanal. 13 (2007) 87.
[29] R. Ma, Y. Dong, L. Xi, S. Yang, Z. Lu, C. Chung, ACS Appl. Mater. Interfaces 5 (2013) 892.
[30] B.S. Allimi, S.P. Alpay, C.K. Xie, B.O. Wells, J.I. Budnick, D.M. Pease, Appl. Phys. Lett. 92 (2008) 202105.
[31] X.F. Zhang, K.X. Wang, X. Wei, J.S. Chen, Chem. Mater. 23 (2011) 5290.
[32] J. Haemers, E. Baetens, J. Vennik, Phys. Status Solidi (a) 20 (1973) 381.
[33] J.-G. Zhang, J.M. McGraw, J. Turner, D. Ginley, J. Electrochem. Soc. 144 (1997) 1630.
[34] N. Yabuuchi, M. Sugano, Y. Yamakawa, I. Nakai, K. Sakamoto, H. Muramatsu, S. Komaba, J. Mater. Chem. 21 (2011) 10035.
[35] Y.-L. Shi, M.-F. Shen, S.-D. Xu, Q.-C. Zhuang, L. Jiang, Y.-H. Qiang, Solid State Ionics 222–223 (2012) 23.
[36] D. Zhang, B.S. Haran, A. Durairajan, R.E. White, Y. Podrazhansky, B.N. Popov, J. Power Sources 91 (2000) 122.
[37] B. Markovsky, M.D. Levi, D. Aurbach, Electrochim. Acta 43 (1998) 2287.
[38] A.J. Gmitter, F. Badway, S. Rangan, R.A. Bartynski, A. Halajko, N. Pereira, G.G. Amatucci, J. Mater. Chem. 20 (2010) 4149.
[39] B. Das, M.V. Reddy, B.V.R. Chowdari, J. Alloys Compd. 565 (2013) 90.
[40] S.S. Zhang, K. Xu, T.R. Jow, Electrochim. Acta 49 (2004) 1057.